Available online at www.sciencedirect.com
ScienceDirect
International Journal of Heat and Mass Transfer 51 (2008) 1238–1250
International Journal of HEAT and MASS TRANSFER
www.elsevier.com/locate/ijhmt

Numerical investigation into the effects of wall roughness on a gas–particle flow in a 90° bend

Z.F. Tian [a], K. Inthavong [a], J.Y. Tu [a,*], G.H. Yeoh [b]

[a] School of Aerospace, Mechanical and Manufacturing Engineering, RMIT University, P.O. Box 71, Bundoora Vic 3083, Australia
[b] Australian Nuclear Science and Technology Organisation (ANSTO), PMB 1, Menai, NSW 2234, Australia

Received 29 November 2006; received in revised form 26 November 2007
Available online 31 January 2008

Abstract

This paper presents a numerical study of a dilute gas–particle flow in a 90° bend by employing a Lagrangian particle-tracking model combined with a particle–wall collision model and a stochastic wall roughness model. The major objective of this study was to investigate the effects of wall roughness on the particle flow properties. The numerical simulation revealed that wall roughness significantly reduced the 'particle free zone' and smoothed the particle number density profiles by altering the particle rebounding behaviours. It was also found that wall roughness reduced the particle mean velocities and also increased the particle fluctuating velocities in both streamwise and transverse directions.

Keywords: Gas–particle flow; 90° bend; CFD; Particle–wall collision; Wall roughness

1. Introduction

Gas–particle flows inside of pipe bends are found in many engineering applications. Air–coal flows in coal combustion equipments, coal liquefaction–gasification in pipe systems, gas–particle flows in turbo machinery, and contaminant particle flows in ventilation ducts are some typical examples. With the significant advancement of computer speed and memory, computational fluid dynamics (CFD) is becoming a viable tool to provide detailed information of both gas and particle phases in the components composing these systems.

For the CFD approach, the particle–wall collision model has an important influence on the prediction of gas–particle flows, especially for relatively large particles [1]. Nevertheless, despite the experimental and computational investigations reported in [1–8] and many others, the success in properly modelling the particle–wall collision process remains elusive due to its complex nature.

Among the parameters, such as the particle incident velocity, incident angle, diameter of particle and its material properties, the wall surface roughness is one of the physical parameters that govern the particle–wall collision process and the wall collision frequency [5]. Sommerfeld and Huber [5] measured the gas–particle flows in a horizontal channel using particle-tracking velocimetry. They found that wall roughness considerably alters the particle rebound behaviour and on average causes a re-dispersion of the particle by reducing the gravitational settling. Another contribution to this work was the development and validation of a stochastic wall roughness distribution model that takes into consideration the so-called shadow effect for small particle incident angles. It was demonstrated that particles may not hit the lee side of a roughness structure when the absolute value of the negative inclination angle $|\gamma_-|$ becomes larger than the impact angle [5]. This results in a higher probability for the particle to hit the luff side, effectively shifting the probability distribution function of the effective roughness angle towards positive values. Later, Kussin and Sommerfeld [6] conducted detailed measurements of gas–particle horizontal channel

* Corresponding author. Tel.: +61 3 99256191; fax: +61 3 99256108.
E-mail address: Jiyuan.Tu@rmit.edu.au (J.Y. Tu).

0017-9310/$ - see front matter © 2007 Elsevier Ltd. All rights reserved.
doi:10.1016/j.ijheatmasstransfer.2007.12.005

Nomenclature

a_1, a_2, a_3	empirical const ants in Eq. (4)
C_D	particle drag coefficient
D	width of the bend
d_p	particle diameter
e_n	mean normal restitution coefficient
g	gravitational acceleration
r_i	inner wall radius
r_o	outer wall radius
r^*	non-dimensional wall distance
Re	Reynolds number
Re_p	relative Reynolds number
St	Stokes number
t_p	particle relaxation time
t_s	system response time
U_b	bulk velocity
u_n^p, v_n^p	particle normal incident velocity and normal reflected velocity
u_t^p, v_t^p	particle tangential incident velocity and tangential reflected velocity
V_s	characteristic velocity of the system

Greek symbols

μ	dynamic viscosity
θ, θ'	the particle incident angle without and with roughness effect
ρ	density
ω, Ω	particle annular velocity before and after collision
ζ	normally distributed random number

Subscripts

g	gas phase
n	normal direction
t	tangential direction
p	particle phase
s	system

Superscript

g	gas phase
p	particle phase
$()'$	fluctuation

flows using glass particles with diameters from 60 μm to 1000 μm and two stainless steel walls with different degrees of wall roughness. It was found that irregular particle–wall collision due to the roughness enhances the transverse dispersion of the particles across the channel and that the wall collision frequency is increased due to a reduction in the mean free path. The wall roughness was also found to decrease the particle mean velocity that is associated with a higher momentum loss in the particle phase while increasing both the streamwise and transverse fluctuating velocities. The effects of wall roughness on particle velocities in a fully developed downward channel flow in air was experimentally investigated by Benson et al. [7], employing a laser Doppler anemometer (LDA) system. Similar to the studies by Kussin and Sommerfeld [6], the wall roughness was found to substantially reduce the streamwise particle velocities causing the particles to be uniformly distributed across the channel after wall collision. The wall roughness also increases the particle fluctuating velocities by nearly 100% near the channel centerplane. Using a stochastic wall roughness model similar to that of Sommerfeld and Huber [5], Squires and Simonin [8] numerically studied the particle phase properties in a gas–particle channel flow with three wall roughness angles, 0° (smooth wall), 2.5° and 5°. The most pronounced effect of wall roughness was found on the wall-normal component of the particle velocity (the transverse particle velocity). The streamwise particle velocity variance was increased, while the transverse particle fluctuating velocity was less sensitive to the wall roughness.

The main focus of this paper is to numerically investigate the effects of wall roughness on the particle–wall collision phenomenon and to extend these ideas to further characterize the particle phase flow in a 90° bend. Previously, Tu and Fletcher [9] computed a gas–particle flow in a square-sectioned 90° bend via an Eulerian–Eulerian model. This two-fluid model, implemented the *Re*-Normalisation Group (RNG) k–ε model along with generalised wall boundary conditions and a particle–wall collision model to better represent the particle–wall momentum transfer. Comparisons of both gas and particle phase velocity computations against Laser Doppler Anemometry (LDA) measurements of Kliafa and Holt [10] were reasonably good. However, the inherent weakness of the Eulerian formulation is its inability to capture the aerodynamic drag force on the particle phase in the vicinity of a wall surface. The incident and reflected particles during the process of a particle–wall collision in the Eulerian model is still far from adequate in terms of resolution [11]. To overcome these difficulties, the Lagrangian particle-tracking is thereby revisited to fundamentally describe the near-wall particle collision process.

The authors [12] used a Lagrangian particle-tracking model, which included the stochastic wall roughness model of Sommerfeld [1], to numerically simulate a gas–particle flow over a tube bank. The predicted mean velocities and fluctuations for both gas and 93 μm particles were validated against experimental data with good agreements. The numerical predictions revealed that the wall roughness has a considerable effect by altering the rebounding behaviours of the large particles, consequently affecting the particle motion downstream and shifting the particle collision frequency distribution on the tubes.

This study employed the Lagrangian model, while including a particle–wall collision model and a stochastic wall roughness model [5] to study the effects of wall rough-

ness on the particle phase flow field in a two-dimensional 90° bend. The aforementioned models were implemented into the FLUENT code via user-defined subroutines. Using user-defined subroutines allows the flexibility in extending the collision model to handle complex engineering flows. To gain confidence in this numerical study, the predicted mean velocities for both gas phase and 50 μm particles were validated against experimental data of Kliafa and Holt [10]. The Lagrangian model was used to investigate effects of wall roughness on the particle trajectories, particle number density distribution, particle mean velocities and particle fluctuating velocities.

2. Computational method

2.1. Gas phase and particle phase modelling

The generic CFD commercial code, FLUENT [13], was utilised to predict the continuum gas phase of the velocity profiles under steady-state conditions. The air phase turbulence was handled by the RNG k–ε model [14].

A Lagrangian-formulated particle equation of motion was solved with the trajectory of a discrete particle phase determined by integrating the force balance on the particle, which is written in a Lagrangian reference frame. Appropriate forces such as the drag and gravitational forces are incorporated into the equation of motion. The equation can be written as

$$\frac{\mathrm{d}u_\mathrm{p}}{\mathrm{d}t} = F_\mathrm{D}(u_\mathrm{g} - u_\mathrm{p}) + \frac{g(\rho_\mathrm{p} - \rho_\mathrm{g})}{\rho_\mathrm{p}} \tag{1}$$

where u is the velocity, ρ is density, g is the gravitational acceleration and the subscript g and p denote the gas and particle phase parameters, respectively. $F_\mathrm{D}(u_\mathrm{g} - u_\mathrm{p})$ is the drag force per unit particle mass, and F_D is given by

$$F_\mathrm{D} = \frac{18\mu_\mathrm{g}}{\rho_\mathrm{p} d_\mathrm{p}^2}\frac{C_\mathrm{D} Re_\mathrm{p}}{24} \tag{2}$$

where μ_g is gas phase dynamic viscosity. Re_p is the relative Reynolds number defined as

$$Re_\mathrm{p} = \frac{\rho_\mathrm{p} d_\mathrm{p} |u_\mathrm{p} - u_\mathrm{g}|}{\mu_\mathrm{g}} \tag{3}$$

d_p is the particle diameter. The drag coefficient C_D is given as

$$C_\mathrm{D} = a_1 + \frac{a_2}{Re_\mathrm{p}} + \frac{a_3}{Re_\mathrm{p}^2} \tag{4}$$

where the a's are empirical constants for smooth spherical particles over several ranges of particle Reynolds number [15]. By using stochastic tracking method as part of the Eulerian–Lagrangian approach, FLUENT predicts the turbulent dispersion of particles by integrating the trajectory equations for individual particles, using the instantaneous fluid velocity, $u_\mathrm{i}^\mathrm{g} + u_\mathrm{i}'(t)$ along the particle path during the integration process. With this method, discrete random walk or "eddy lifetime" model, is applied where the fluctuating velocity components, u_i' that prevail during the lifetime of the turbulent eddy are sampled by assuming that they obey a Gaussian probability distribution, so that

$$u_\mathrm{i}' = \xi\sqrt{\overline{u_\mathrm{i}'^2}} \tag{5}$$

where ξ is a normally distributed random number, and the remaining right-hand side is the local root mean square (rms) velocity fluctuations that can be obtained (assuming isotropy) by

$$\sqrt{\overline{u_\mathrm{i}'^2}} = \sqrt{2k_\mathrm{g}/3} \tag{6}$$

The interaction time between the particles and eddies is the smaller of the eddy lifetime, τ_e and the particle eddy crossing time, t_cross. The characteristic lifetime of the eddy is defined as

$$\tau_\mathrm{e} = -T_\mathrm{L}\log(r) \tag{7}$$

where T_L is the fluid Lagrangian integral time, $T_\mathrm{L} \approx 0.15/\omega$. The variable r is a uniform random number between 0 and 1. The particle eddy crossing time is given by

$$t_\mathrm{cross} = -t_\mathrm{p}\ln\left[1 - \left(\frac{Le}{t_\mathrm{p}|u_\mathrm{i}^\mathrm{g} - u_\mathrm{i}^\mathrm{p}|}\right)\right] \tag{8}$$

where t_p is the particle relaxation time ($= \rho_\mathrm{s} d_\mathrm{p}^2/18\rho_\mathrm{g} v_\mathrm{g}$), Le is the eddy length scale, and $|u_\mathrm{i}^\mathrm{g} - u_\mathrm{i}^\mathrm{p}|$ is the magnitude of the relative velocity. The particle interacts with the fluid eddy over the interaction time. When the eddy lifetime is reached, a new value of the instantaneous velocity is obtained by applying a new value of ξ in Eq. (5).

The main focus of this paper is the effects of wall roughness on the particle phase flow field therefore, the volume fraction of particle phase was assumed to be very low ($\leqslant 10^{-6}$). According to Elghobashi [16], the particles do not influence the carrier phase when the particle phase volume fraction is less than 10^{-6} and the flow is in the limit of one-way coupling.

2.2. The particle–wall collision model and wall roughness model

The particle–wall collision model of Sommerfeld and Huber [5] was employed to account for the particle–wall interaction process. Fig. 1 illustrates the impact of a spher-

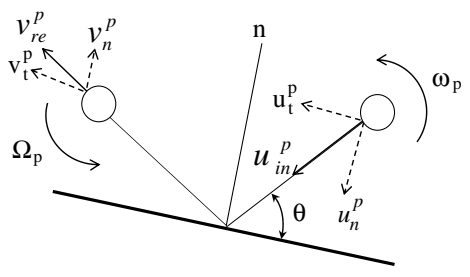

Fig. 1. Particle–wall collision configuration.

ical particle on a plane wall in two-dimensional form. At the end of contact with a wall, a particle is considered rolling when the following conditioned is satisfied:

$$\left|u_t^p - \frac{d_p}{2}\omega_p\right| \leqslant \frac{7}{2}\mu_d(1+e_n)u_n^p \tag{9}$$

The subscript n and t represents the normal and tangential velocity components, respectively. μ_d is the particle dynamic friction coefficient, ω_p denotes the particle incident angular velocity and e_n is the kinematic restitution coefficient that can be expressed as

$$e_n = -v_n^p/u_n^p \tag{10}$$

where u_n^p is the normal incident velocity and v_n^p is the normal reflected velocity.

Under conditions of rolling collision, the rebounding velocity components are as follows:

$$\begin{aligned} v_t^p &= \frac{1}{7}(5u_t^p + d_p\omega_p) \\ v_n^p &= -e_n u_n^p \\ \Omega_p &= 2\frac{v_t^p}{d_p} \end{aligned} \tag{11}$$

where Ω_p is particle rebound angular velocity.

If Eq. (9) is not satisfied, the particle is then considered to be sliding and the rebound velocity components are defined as

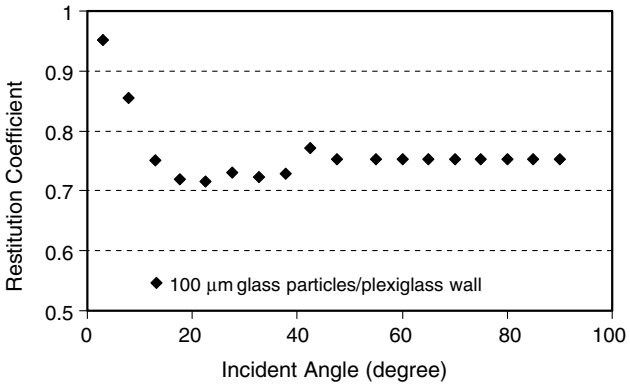

Fig. 2. Restitution coefficient of 100 μm glass particles collision on plexiglass wall [5].

$$\begin{aligned} v_t^p &= u_t^p - \mu_d(1+e_n)\varepsilon_0 u_n^p \\ v_n^p &= -e_n u_n^p \\ \Omega_p &= \omega_p + 5\mu_d(1+e_n)\varepsilon_0\frac{u_n^p}{d_p} \end{aligned} \tag{12}$$

here ε_0 is the direction of the relative velocity between particle surface and wall, obtained by

$$\varepsilon_0 = \mathrm{sign}\left(u_t^p - \frac{d_p}{2}\omega_p\right) \tag{13}$$

The values for the restitution coefficient e_n and the dynamic friction coefficient μ_d are obtained from experiments. In this study, e_n and μ_d were calculated based on the constants of 100 μm glass particles impacting on a plexiglass surface [5]. The measured restitution coefficient e_n was measured

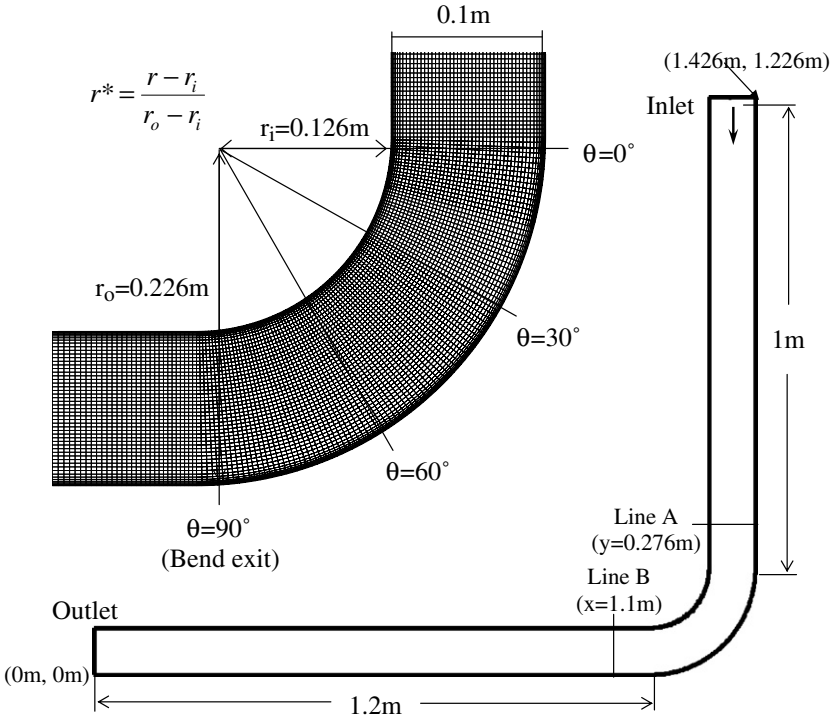

Fig. 3. Computational domain and grids of a two-dimensional 90° bend.

for incident angles up to 40°, thus values of e_n above 40° were assumed to have the same value as e_n at 40°. Fig. 2 gives the restitution coefficient e_n of 100 μm glass particles collision on plexiglass wall used in this study. The dynamic friction coefficient μ_d was 0.15.

A stochastic approach has been developed by Sommerfeld [1] to take into consideration the wall roughness effect. Here, the incident angle α_1' comprises of the particle incident angle α_1 and a stochastic contribution due to the wall roughness, viz.

$$\alpha_1' = \alpha_1 + \Delta\gamma\xi \tag{14}$$

From the above, ξ is a Gaussian random variable with mean of 0 and a standard deviation of 1. The value of $\Delta\gamma$ is determined through experiments.

When the absolute value of the negative $\Delta\gamma\xi$ is larger than the incident angle, particles may not impact on the *lee* side of a roughness structure. This phenomenon is known as the shadow which leads to a higher probability of particles colliding on the *luff* side, causing a shift of the probability distribution function of $\Delta\gamma\xi$ towards positive values. The method proposed by Sommerfeld and Huber [5] is implemented in this study to handle the shadow effect. This procedure allows for the positive shift of the distribution function of $\Delta\gamma\xi$ thus avoiding the unphysical situation where particles hit the roughness structure with a negative angle. In this study, the wall roughness angles of 0°, 2.5° and 5° was used. More details about the wall roughness model can be found in Sommerfeld and Huber [5].

2.3. Numerical procedure

The non-equilibrium wall function was employed for the gas phase flow because of its capability to better handle complex flows where the mean flow and turbulence are subjected to severe pressure gradients and rapid change, such as separation, reattachment and impingement. The governing transport equations were discretised using the finite-volume approach and the QUICK scheme was used to approximate the convective terms while the second-order accurate central difference scheme is adopted for the diffusion terms. The

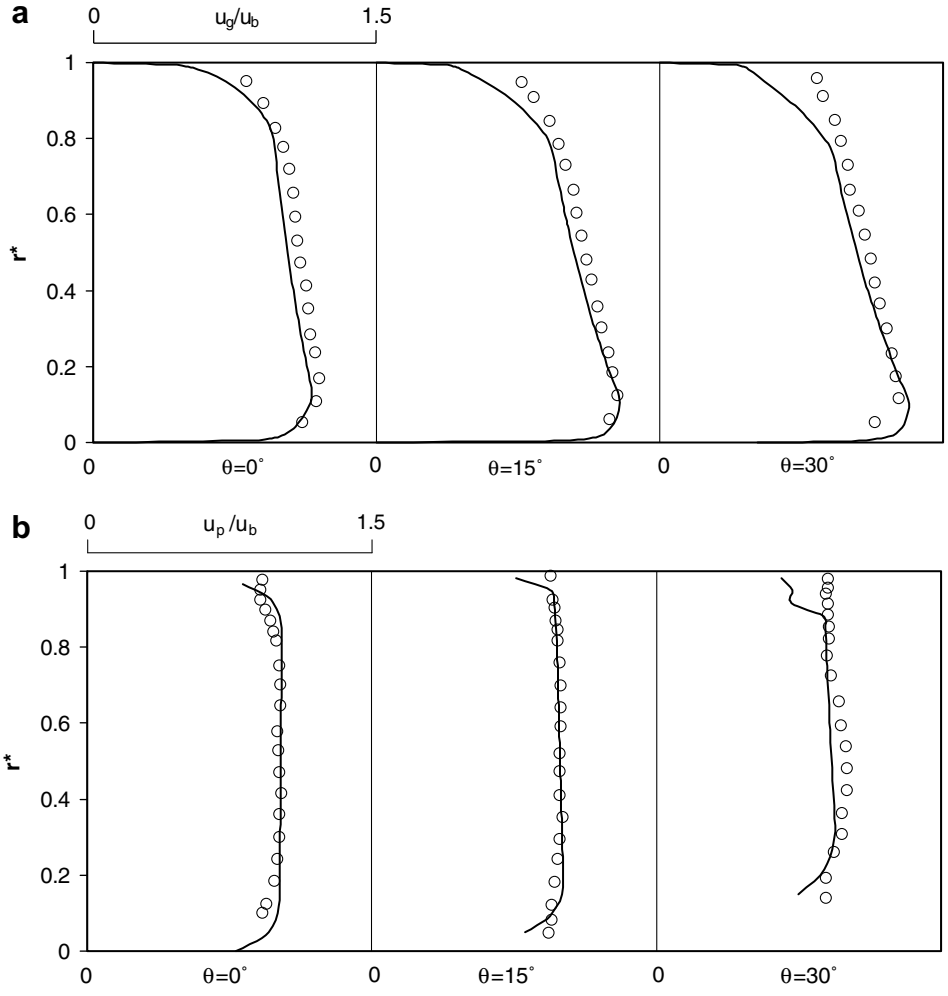

Fig. 4. Comparison between the experimental data and numerical simulation: (a) gas phase streamwise velocity, (b) particle phase streamwise velocity ($U_b = 52.19$ m/s, 50 μm particle). *Circles*: experimental data, *line*: prediction.

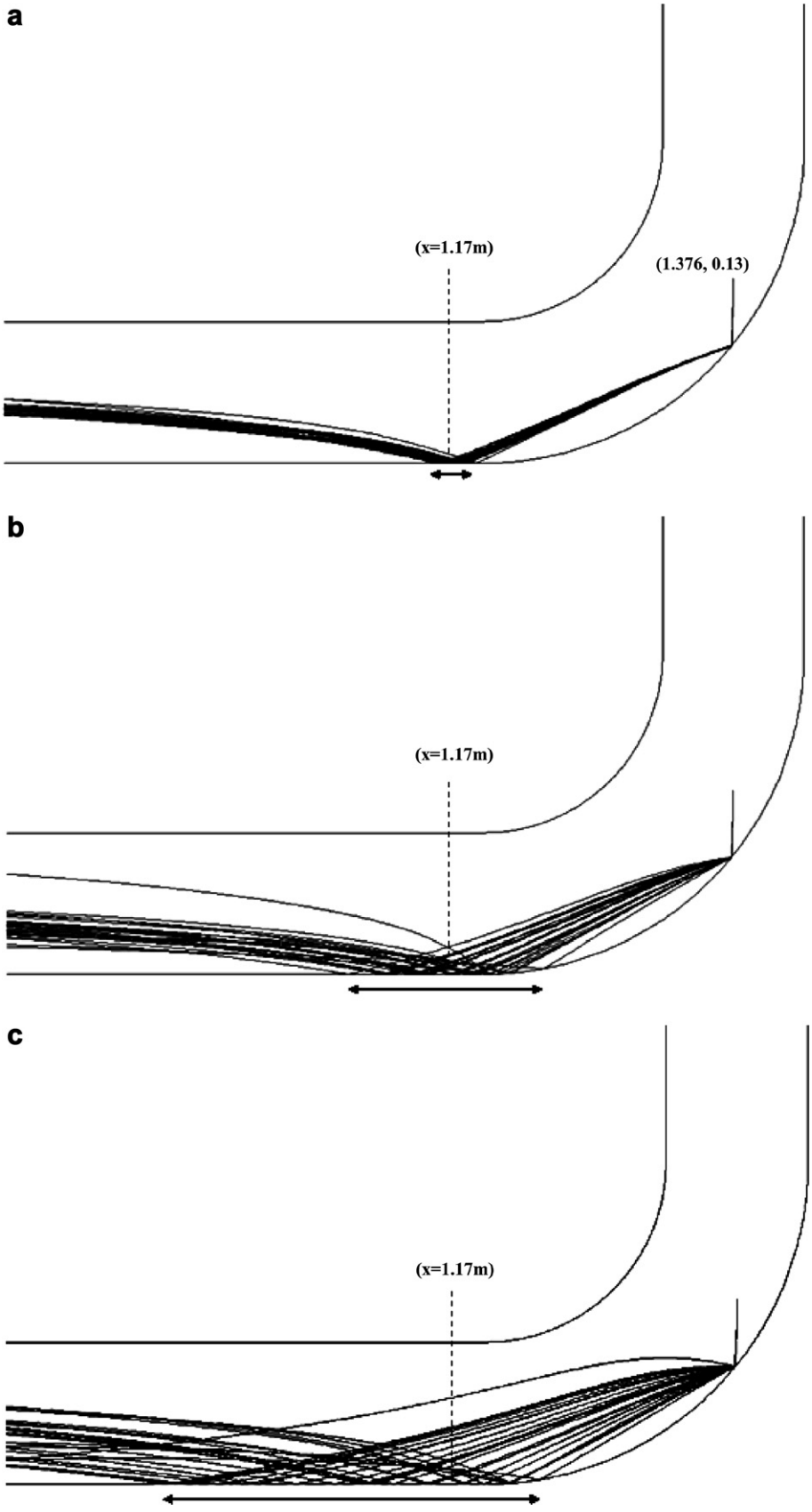

Fig. 5. Computed trajectories for 100 μm particles released at (1.376, 0.16) with different wall roughness angle: (a) 0°, (b) 2.5° and (c) 5°. ↔ represents the length of the second collision region ($U_b = 10$ m/s, $Re = 6.65 \times 10^4$).

pressure–velocity coupling was realized through the SIMPLE method and the convergence criteria for the gas phase properties were assumed to have been met when the iteration residuals had reduced by five orders of magnitude.

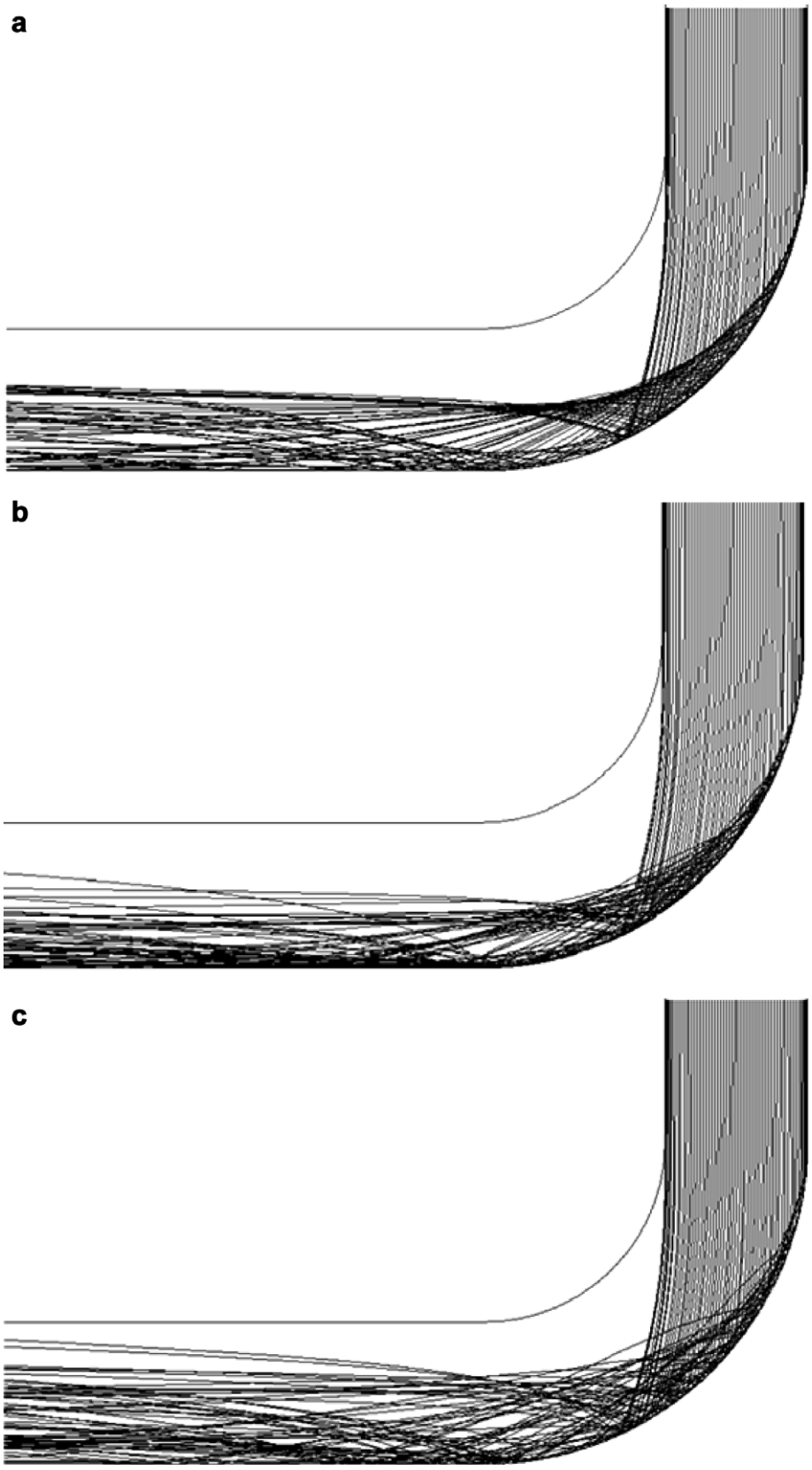

Fig. 6. Computed trajectories for particles released at 1D before the bend with different wall roughness angle: (a) 0°, (b) 2.5° and (c) 5° ($U_b = 10$ m/s, $Re = 6.65 \times 10^4$).

The governing equations for the gas phase were initially solved towards steady state. The Lagrangian solution for the particle phase was thereafter achieved by the injection of particles into the bulk gas flow where the trajectories of each particle were determined from the steady-state gas phase results. For gas–particle flows in bends, the secondary flow and side walls may impose significant influence on particle phase properties such as the particle number density (particle concentration) distribution, particle mean velocities and particle fluctuating velocity. In order to analyze the effect of the wall roughness on particle phase field independent of the effects from the secondary flow and side wall, the current study was simulated in a two-dimensional bend. For the same reason of simplicity, particles were assumed to be spherical and mono-sized.

3. Results and discussion

Fig. 3 shows the computational domain where the inlet begins 1 m upstream from the bend entrance and extends 1.2 m downstream from the bend exit. The bend has an inner radius (r_i) of 0. 126 m and an outer radius (r_o) of 0.226 m for the outer wall. The results were plotted against a non-dimensional wall distance $r^* = \frac{r-r_i}{r_o-r_i}$. Within the 1 m long channel before the bend, 380 (in the streamwise direction) × 58 (in the transverse direction) grid points have been allocated. In the bend, the mesh is with 168 grid points in the streamwise direction and 58 grid points in the transverse direction. The 1.2 m long channel after the bend has a 450 (in the streamwise direction) × 58 (in the lateral direction) grid mesh. Grid independence was checked by refining the mesh system by a mesh density of 1122 (in the streamwise direction) × 68 (in the transverse direction) grid points. Simulations of 10 m/s case revealed that the difference of the velocity profile between the two mesh schemes at $\theta = 0°$ is less than 3%. The coarser mesh was therefore applied in order to embrace the increase of computational efficiency towards achieving the final results. Part of the mesh of 998 × 58 grid mesh is illustrated in Fig. 3.

To gain confidence in this computational study, experimental measurements for a gas–particle flow with the same bend configuration as this study but three-dimensional [10] was used to validate the simulations. In this validation case, the gas phase bulk velocity was 52.19 m/s corresponding to the Reynolds number of 3.47×10^5 (based on the bend width of 0.1 m). A total of 100,000 glass particles (material density 2990 kg/m^3) with a diameter of 50 μm were released from 100 uniformly distributed points across the inlet surface, were individually tracked within the computational domain. The particle inlet velocity for this validation case was 52.19 m/s. The restitution coefficient e_n of the glass particle collision on the plexiglass surface [5] was used and the wall roughness degree was 3.8°.

Fig. 4a shows the comparison between the measured and predicted streamwise gas velocities normalised by the

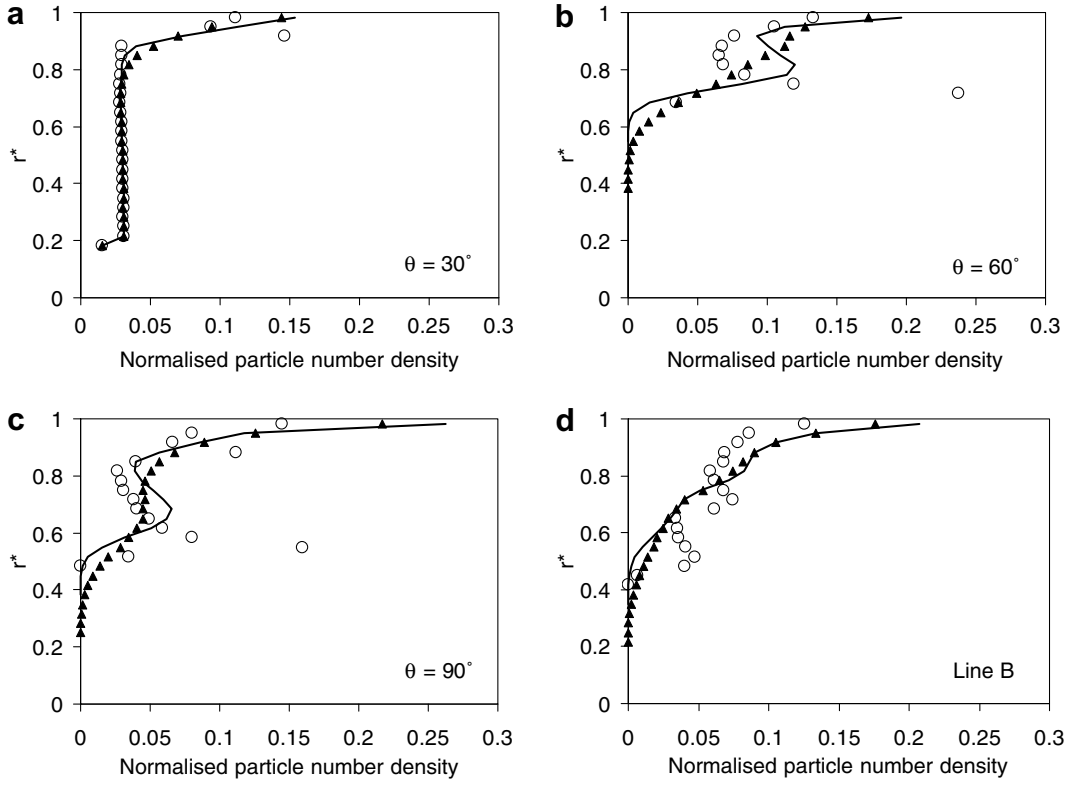

Fig. 7. Computed particle number concentration with different wall roughness angles: (a) at $\theta = 30°$, (b) at $\theta = 60°$, (c) at $\theta = 90°$, (d) at Line B. *Circles*: 0° roughness, *line*: 2.5° roughness, *solid triangle*: 5° roughness ($U_b = 10$ m/s, $Re = 6.65 \times 10^4$).

bulk velocity at $\theta = 0°$, 15° and 30° angles within the bend section. The numerical simulation successfully predicted the flow acceleration of the gas phase near the inner wall region ($r^* \sim 0$). In the region near the outer wall ($r^* \sim 1$), the fluid deceleration caused by the unfavorable pressure gradient was also captured. The predicted gas phase velocity is in good agreement with the measurement (within 10%) except for an under prediction of up to (35%) observed in the outer wall region at $\theta = 30°$. Fig. 4b presents the normalised velocity profile of 50 μm particles at $\theta = 0°$, 15° and 30° stations. The predictions and measurements showed good agreement (within 10 %) while there is an under-prediction of up to 20% in the outer wall region at $\theta = 30°$.

To investigate the effects of wall roughness on the particle phase flow field in the bend, glass particles with corresponding diameters of 100 μm were simulated under the flow condition of 10 m/s. The corresponding Reynolds number based on the bend width of 0.1 m was 6.65×10^4. Note that the flow condition now uses an inlet velocity of 10 m/s which is more likely to be found in real engineering applications.

3.1. Effects of wall roughness on particle trajectories

The influence of wall roughness on the particle trajectories was firstly investigated by tracking 25 particles released from a point location at (1.376, 0.13). For qualitative purposes only a small number of particles are used as this allows particle-tracking to be performed graphically without smearing of the results due to the overloading of lines associated with a large number of particles being graphically tracked. Fig. 5a illustrates the particle trajectories with 0° wall roughness angle. All the particles rebounding from the first collision followed very similar trajectories which consequently produced a narrow secondary collision zone. The center of this secondary collision zone is located about 0.3D after the bend ($x = 1.17$ m). When the wall roughness angle was increased, the behaviours of particles were markedly different. The particles were observed to

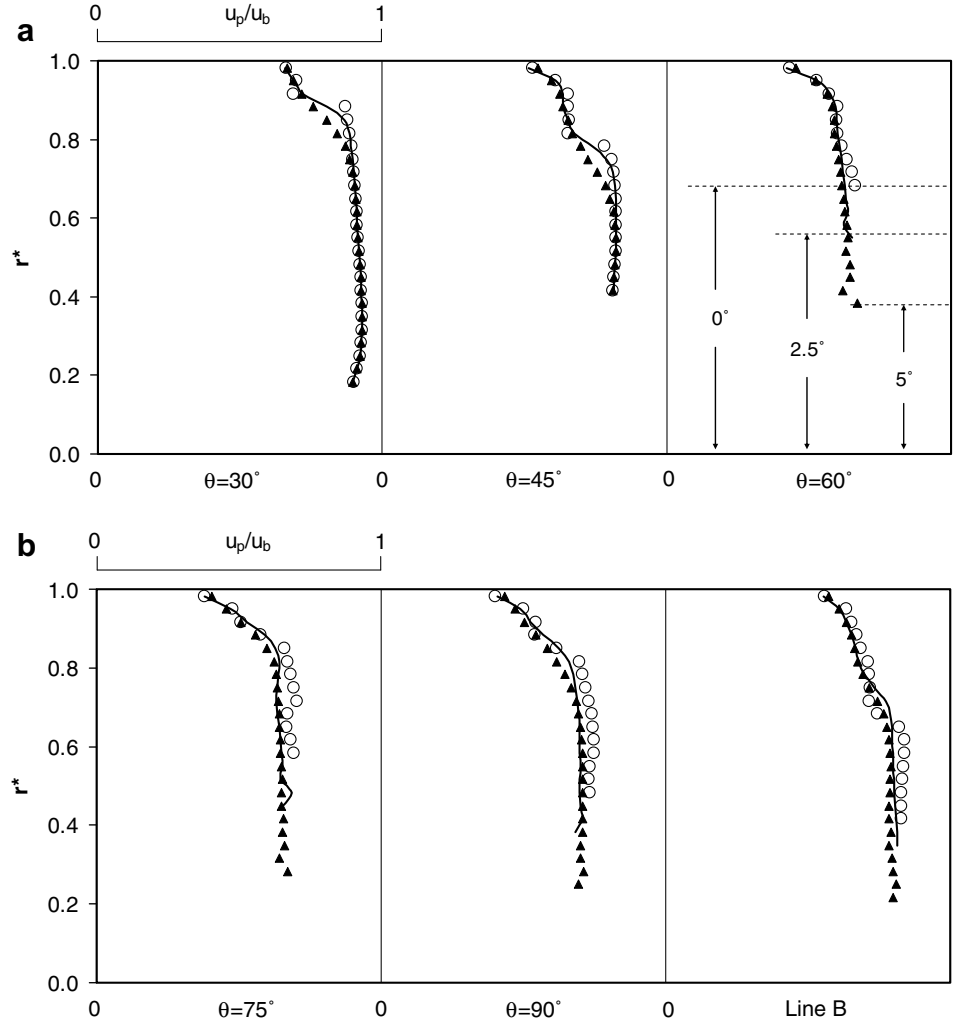

Fig. 8. Comparison of particle streamwise mean velocity profiles with different roughness angles at different locations. ↔ The length of the particle free zone. *Circles*: 0° roughness, *line*: 2.5° roughness, *solid triangle*: 5° roughness ($U_b = 10$ m/s, $Re = 6.65 \times 10^4$).

rebound in many directions caused by an increase in the randomness from the rebounding of a rougher wall surface. A wider dispersion of particles was observed, leading to a significant increase in the second collision zone length. An increase of almost 4 times for the case of a 2.5° roughness angle was found in Fig. 5b, while an increase of 10 times was found for 5° roughness angle in Fig. 5c. A closer investigation for the 5° roughness angle, revealed that the secondary collision zone contained more particles impacting to the left of $x = 1.17$ m, which is the secondary collision zone location for 0° roughness. It should be noted that there exists a significant contribution from the particles inertia on the particle trajectory after the first collision. The increase in wall roughness causes a wider re-dispersion of particles, and thus this new trajectory, coupled with a high inertia results in the negligible influences from the bulk fluid. This allows the particles to travel further to the left, causing a wider secondary collision zone.

In Fig. 5a, the small deviation of particle trajectories after the first collision is attributed to the gas phase turbulence. For gas–particle flows, the dimensionless Stokes number, $St = t_p/t_s$, represents an important criteria towards better understanding the state of the particles in determining whether they are in kinetic equilibrium with the surrounding gas or not. The system relaxation time t_s in the Stokes number is determined from the characteristic length ($L_s = D = 0.1$ m) and the characteristic velocity ($U_b = 10$ m/s) for the system under investigation, i.e. $t_s = L_s/U_b$. For the case of 100 μm particle, the Stokes number is equal to 9, much greater than unity. Therefore, the influence from the gas phase turbulence on the 100 μm particle trajectories is negligible in comparison with the influence from the wall roughness as shown in Fig. 5b and c.

To further investigate the effects of wall roughness on the particle trajectories, 58 particles with streamwise velocity of 10 m/s were released from Line A as shown in Fig. 3 ($y = 0.276$ m), which is located 1D upstream from the bend entrance. Fig. 6a–c shows the particle trajectories in the bend for different wall roughness angles, i.e., 0°, 2.5° and 5°, respectively. With the increase of the wall roughness angle, the 'particle free zone' occurring at the inner wall region is reduced as the wall roughness increases. For the 5° case, particles were found to disperse further into the upper region of the channel after the bend, following the first collision. This same region is observed to be a 'particle free zone' for the 0° case.

3.2. Effects of wall roughness on particle number density

To investigate the influence of wall roughness on the particle dispersion, the particle number density distribution taken along different sections around the bend is used. To obtain statistically meaningful results a larger number of particles is now used where 100,000 mono-sized particles (100 μm) with streamwise velocity of 10 m/s were released from 100 uniformly distributed points across Line A. The independence of statistical particle phase prediction from the increase of the number of particles used was tested by implementing 50,000, 100,000 and 200,000 particles. The difference of the particle phase velocities at $\theta = 0°$ of

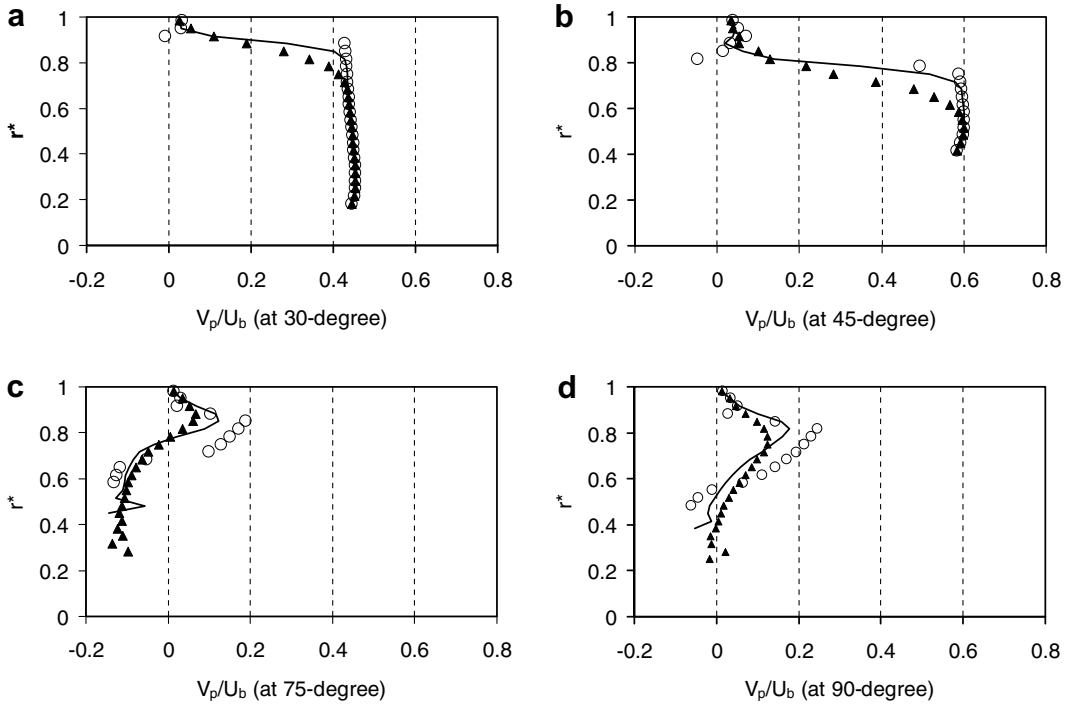

Fig. 9. Comparison of particle transverse mean velocity profiles with different roughness angles at different locations. *Circles*: 0° roughness, *line*: 2.5° roughness, *solid triangle*: 5° roughness ($U_b = 10$ m/s, $Re = 6.65 \times 10^4$).

50,000 and 100,000 particles was less than 3% and for 100,000–200,000 was less than 1%, thus in terms of computational efficiency 100,000 particles was used hereafter.

The particle number density normalised by the number of inlet particles, 100,000 at $\theta = 30°$ with different wall roughness angles, are presented in Fig. 7a. The particle distribution profiles in this case for the three wall roughness angles are very similar. A much higher particle number density for all roughness angles is found near the outer wall region and this phenomenon is consistent with the observations from the experimental study of [10] and the Eulerian–Eulerian simulation of [9]. With the turning of the bend from $\theta = 30°$ to $\theta = 60°$ the trend for particle number density sees an increase in the outer region from $r^* = 0.65$ to $r^* = 0.9$ for all wall roughness angles and a decrease in the region from $r^* = 0.4$ to $r^* = 0.45$ for roughness angle of 5°. No particles are found in the inner wall region (from $r^* = 0$ to $r^* = 0.4$). This is due to the high inertia of 100 μm particles, which causes particles to respond slowly to the local gas phase changes. At $\theta = 60°$, an interesting phenomenon is found for the 0° wall roughness case where two local maximus for particle number density are observed at the region at $r^* = 0.75$ and in the outer wall region. The prediction of high particle number density in the middle bend region was not found either in the experimental study of [10] or in the Eulerian–Eulerian simulation of [9]. This non-physical phenomenon is remedied when the wall roughness is taken into consideration. The high particle number density at $r^* = 0.75$ is reduced dramatically when the wall roughness was increased to 2.5°. A further increase to 5°, showed a smoother particle number density profile, suggesting a greater dispersion of particles being distributed over a greater area within the bend. This leads to a significant decrease in the 'particle free zone'. However, the total number of particles in the region from $r^* = 0.4$ to $r^* = 0.55$ is about 2000 which accounts for 2% of the total particles tracked whereas high particle number densities are found in the region next to the outer wall for all roughness angles. A similar phenomenon is found at $\theta =$ 90°, the high particle number density at $r^* = 0.6$ is found in the 0° wall roughness case. With the increase of wall roughness angles, the high particle density at this

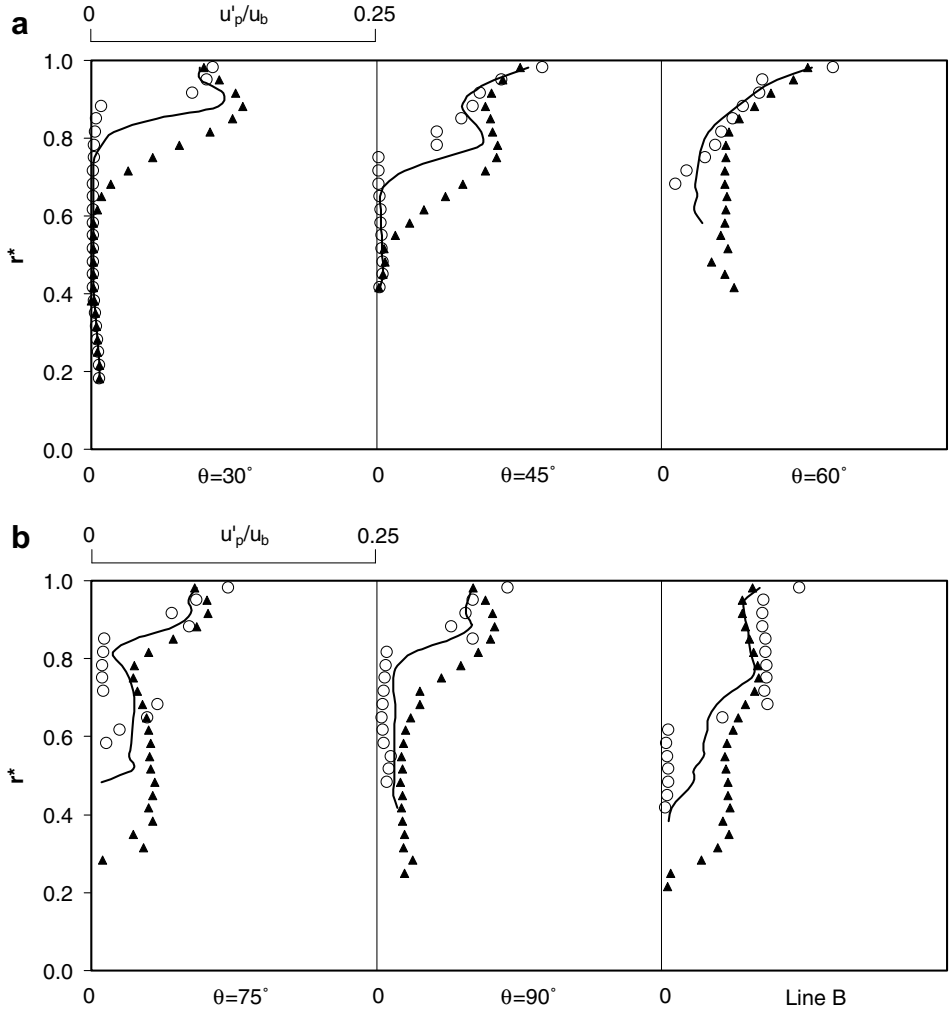

Fig. 10. Comparison of particle streamwise rms fluctuation velocity profiles with different roughness angles at different locations. *Circles*: 0° roughness, *line*: 2.5° roughness, *solid triangle*: 5° roughness ($U_b = 10$ m/s, $Re = 6.65 \times 10^4$).

region is dramatically reduced. Fig. 7d shows the particle distribution profiles at Line B, 1D after the exit. It is seen that the wall roughness structure enhances the re-dispersion of particles after the first collision leading to the smoother particle number density profile. Additionally, the 'particle free zone' was reduced with an increase in the wall roughness and relatively low particle number densities were observed in the region from $r^* = 0.25$ to $r^* = 0.32$.

3.3. Effects of wall roughness on particle mean velocities

The effects of wall roughness on particle mean velocities at different locations in the bend are shown in Fig. 8. At $\theta = 30°$, the streamwise velocity of 5° roughness is slightly smaller than the 0° case at the outer wall region from $r^* = 0.85$ to $r^* = 0.92$. This is the consequence of particles having collided on the outer wall before 30° and the loss of momentum which is greater for walls with a higher roughness. However, the particle streamwise velocity profiles for the rest of the region is almost identical for all wall roughness, since this region is still in the early stages of the bend and particle collision has not occurred. After $\theta = 60°$, however, the bend curvature is much greater and most particles have experienced the first wall collision resulting in a reduction in the mean streamwise velocities due to the average increase in momentum loss. This can be seen in the comparison of velocity profiles for at $\theta = 0°$ to at $\theta = 60°$ which has shifted to the left. For bend angles, $\theta > 60°$ the mean velocity profiles for 0° wall roughness exhibit larger magnitudes than for 2.5° and 5° wall roughness. The higher wall roughness causes the particles to lose more of its momentum whilst dispersing the particles in greater directions, hence the wider velocity profile, reaching to $r^* = 0.2$ (from the outer wall $r^* = 1$) for 5° roughness, compared with $r^* = 0.4$ for 0° roughness at Line B.

Fig. 9 shows the particle mean transverse velocities at different locations. At $\theta = 30°$, the velocity profiles for different wall roughness angles are almost identical except for the region from $r^* = 0.85$ to $r^* = 0.92$. At $\theta = 45°$, the velocity profile for 5° roughness is much smaller than the 0° roughness profile at the region from $r^* = 0.62$ to $r^* = 0.79$. At $\theta = 75°$, the mean transverse velocities of 2.5° and 5° roughness are identical and slightly smaller than the smooth wall case. This can be attributed to the early collision occurring before $\theta = 45°$. The reduction of this particle mean velocity is consistent with observations that wall roughness reduces the mean particle velocities as obtained by Kussin and Sommerfeld [6] and Benson et al. [7].

3.4. Effects of wall roughness on particle rms fluctuation velocities

Fig. 10 illustrates the distribution of the particle streamwise rms fluctuating velocities for 0°, 2.5° and 5° roughness angles at various locations. As shown in Fig. 10a, the particle rms fluctuation velocity at $\theta = 30°$ for all three roughness angles yielded almost zero turbulence intensities from $r^* = 0.2$ to $r^* = 0.62$. This is attributed to the fact that particle rms fluctuating velocity is zero at the inlet (Line A) and most particles flowing through this region have not collided with the bend yet. Considerably higher particle velocity fluctuations were found in the region near the

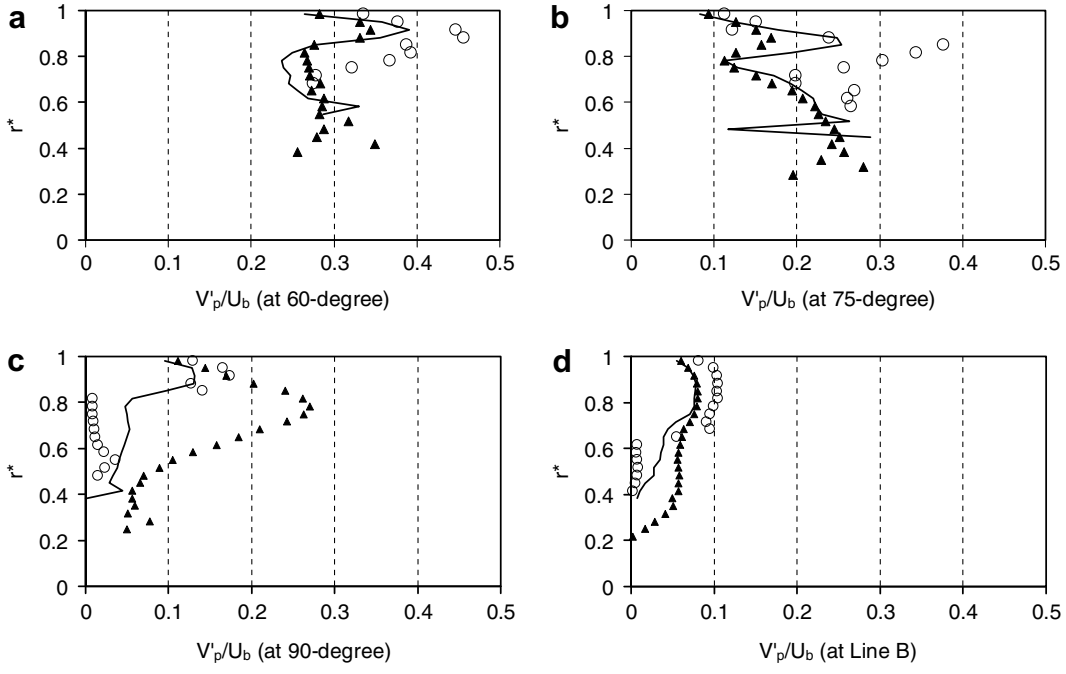

Fig. 11. Comparison of particle transverse rms fluctuation velocity profiles with different roughness angles at different locations. *Circles*: 0° roughness, *line*: 2.5° roughness, *solid triangle*: 5° roughness ($U_b = 10$ m/s, $Re = 6.65 \times 10^4$).

outer wall to $r^* = 0.62$ which is a result of the particle collisions at outer wall. Also, the particle streamwise rms fluctuation velocities of 2.5° and 5° roughness angles are higher than the 0° case, since the wall roughness model enhances the randomness for particle velocities and trajectories after collision. At $\theta = 45°$, the particle streamwise rms fluctuation velocities of 2.5° and 5° roughness angles are higher than the 0° case from $r^* = 0.5$ to $r^* = 0.9$.

The particle transverse rms fluctuation velocities with different wall roughness angles are shown in Fig. 11. An interesting phenomenon can be seen at $\theta = 60°$ where the transverse rms fluctuation velocities for all wall roughness cases are high. This is due to the dominant particle collision which produces a particle rebound velocity that is slightly smaller than the incident velocity due to the momentum lost during the collision process. At $\theta = 90°$, the particle transverse rms fluctuation velocities of 2.5° and 5° roughness angles are higher than the smooth wall case. Figs. 10 and 11 clearly indicate that the wall roughness has a significant influence on the particle velocity fluctuations.

4. Conclusion and future work

The physical behaviours of a dilute gas–particle flow in a 90° bend were numerically investigated via a Lagrangian particle-tracking model. A particle–wall collision model and a stochastic model [5] were adopted to take into consideration the particle–wall collision and wall roughness effect. Good agreements were achieved between the predictions of mean velocity for gas phase and 50 μm particles and experimental data of [10].

A substantial amount of work was taken in this study to elucidate further the understanding of the effect of wall roughness on the flow field of large particles (100 μm). It was found that the wall roughness considerably altered the rebounding behaviours of particles by significantly reducing the 'particle free zone' and smoothing the particle number density profiles. The effects of wall roughness on the particle mean and fluctuating velocities were also investigated. The numerical results confirmed that the particle mean velocities for 2.5° and 5° roughness angles were reduced due to the wall roughness which, on average increases the momentum loss for the particle phase. Also, the particle fluctuating velocities were increased when taking into consideration the wall roughness, since the wall roughness produced greater randomness in the particle rebound velocities and trajectories.

These numerical results suggest that the effect of wall roughness is not negligible for large particles in confined flow geometries such as a 90° bend. Moreover, the particle–wall collision model should account for the effect of wall roughness in order to provide a more realistic description of the particle–wall collision phenomenon. This work will also be beneficial to the understanding and the accurate prediction of gas–particle flows as well as furthering the understanding of the erosion distribution in 90° bends.

Work is in progress to investigate the effects of wall roughness on the particle flow field in three-dimensional bend flows. Additionally, the gas–particle flows investigated in this study were very dilute and particles were unimodel in size (monodisperse). Therefore, future work is still required to assess the effects of wall roughness for dense particle flows and polydisperse particles.

Acknowledgement

The financial support provided by the Australian Research Council (project ID LP0347399) is gratefully acknowledged.

References

[1] M. Sommerfeld, Modelling of particle–wall collisions in confined gas–particle flows, Int. J. Multiphase Flow 18 (6) (1992) 905–926.
[2] S. Matsumoto, S. Saito, Monte Carlo simulation of horizontal pneumatic conveying based on the rough wall model, J. Chem. Eng. Jpn. 3 (1970) 223–230.
[3] G. Grant, W. Tabakoff, Erosion prediction in turbomachinery resulting from environmental solid particles, J. Aircraft 12 (5) (1975) 471–478.
[4] R.M. Brach, P.F. Dunn, Models of rebound and capture for oblique microparticle impact, Aerosol Sci. Technol. 29 (1998) 379–388.
[5] M. Sommerfeld, N. Huber, Experimental analysis and modelling of particle–wall collisions, Int. J. Multiphase Flow 25 (1999) 1457–1489.
[6] J. Kussin, M. Sommerfeld, Experimental studies on particle behaviour and turbulence modification in horizontal channel flow with different wall roughness, Exp. Fluids 33 (2002) 143–159.
[7] M. Benson, T. Tanaka, J.K. Eaton, Effects of wall roughness on particle velocities in a turbulent channel flow, J. Fluids Eng. 127 (2005) 250–256.
[8] K.D. Squires, O. Simonin, LES-DPS of the effect of wall roughness on dispersed phase transport in particle-laden turbulent channel flow, Int. J. Heat Fluid Flow 27 (2006) 619–629.
[9] J.Y. Tu, C.A.J. Fletcher, Numerical computation of turbulent gas–solid particle flow in a 90° bend, AICHE J. 41 (1995) 2187–2197.
[10] Y. Kliafa, M. Holt, LDV measurements of a turbulent air–solid two-phase flow in a 90° bend, Exp. Fluids 5 (1987) 73–85.
[11] Z.F. Tian, J.Y. Tu, G.H. Yeoh, Numerical simulation and validation of dilute gas–particle flow over a backward-facing step, Aerosol Sci. Technol. 39 (2005) 319–332.
[12] Z.F. Tian, J.Y. Tu, G.H. Yeoh, Numerical modelling and validation of gas–particle flow in an in-line tube bank, Comput. Chem. Eng. 31 (2007) 1064–1072.
[13] Fluent User's Guide, Version 6.2., 2005 (Chapters 11 and 23).
[14] V. Yakhot, S.A. Orszag, Renormalization group analysis of turbulence: I. Basic theory, J. Sci. Comput. 1 (1986) 3–51.
[15] S.A. Morsi, A.J. Alexander, Investigation of particle trajectories in 2-phase flow systems, J. Fluid Mech. 55 (1975) 193–208.
[16] S. Elghobashi, On the predicting particle-laden turbulent flows, Appl. Sci. Res. 52 (1994) 309–329.